Nanotribology of Octadecyltrichlorosilane Monolayers and Silicon: Self-Mated versus Unmated Interfaces and Local Packing Density Effects

Erin E. Flater,[†,‡] W. Robert Ashurst,[§] and Robert W. Carpick*[,†,#]

Department of Engineering Physics, University of Wisconsin−Madison, Madison, Wisconsin 53706, and Department of Chemical Engineering, Auburn University, Auburn, Alabama 36849

Received December 16, 2006. In Final Form: April 4, 2007

We use atomic force microscopy (AFM) to determine the frictional properties of nanoscale single-asperity contacts involving octadecyltrichlorosilane (OTS) monolayers and silicon. Quantitative AFM measurements in the wearless regime are performed using both uncoated and OTS-coated silicon AFM tips in contact with both uncoated and OTS-coated silicon surfaces, providing four pairs of either self-mated or unmated interfaces. Striking differences in the frictional responses of the four pairs of interfaces are found. First, lower friction occurs with OTS present on either the tip or substrate, and friction is yet lower when OTS is present on both. Second, the shape of the friction versus load plot strongly depends on whether the substrate is coated with OTS, regardless of whether the tip is coated. Uncoated substrates exhibit the common sublinear dependence, consistent with friction being directly proportional to the area of contact. However, coated substrates exhibit an unusual superlinear dependence. These results can be explained qualitatively by invoking molecular plowing as a significant contribution to the frictional behavior of OTS. Direct in situ comparison of two intrinsic OTS structural phases on the substrate is also performed. We observe frictional contrast for different local molecular packing densities of the otherwise identical molecules. The phase with lower packing density exhibits higher friction, in agreement with related previous work, but decisively observed here in single, continuous images involving the same molecules. Lateral stiffness measurements show no distinction between the two OTS structural phases, demonstrating that the difference in friction is not due to divergent stiffnesses of the two phases. Therefore, the packing density directly affects the interface's intrinsic resistance to friction, that is, the interfacial shear strength.

Introduction

The tribological study of thin organic coatings is motivated by the desire to improve micro- and nanoelectromechanical system (MEMS/NEMS) technologies, and also to develop a more fundamental understanding of tribology in general. Self-assembled monolayers (SAMs) form spontaneously when a molecular precursor, either in a solution or in a vapor, is exposed to a surface.[1] SAMs are ideal for studying fundamental chemical and physical phenomena since they can be attached to a variety of substrates, they form well-defined and uniform interfaces, and both the head and tail groups can be tailored to study their effects on properties such as adhesion and friction.[2] SAM coatings are important for determining frictional mechanisms because SAMs are tailorable molecularly ordered films.

SAMs with silane head group chemistry allow for passivation of hydrophilic silicon MEMS surfaces and show promise to reduce both adhesion and friction for MEMS interfaces and thus improve device performance.[3−9] Complex devices like MEMS typically have some degree of nanometer-scale surface roughness, which causes the interface to be composed of multiple asperity contacts. Assessing the fundamental contributions to friction and wear is therefore facilitated by considering the tribological properties of nanoscale single asperities.

Previous studies of the nanotribological properties of SAMs have elucidated several mechanisms that affect their frictional behavior, a few of which are summarized in references 10 and 11. In general, the total static frictional force F_f is a measure of the resistance of two sliding bodies in contact and may arise from multiple sources:

$$F_f = F_i + F_p + F_v + \cdots \quad (1)$$

where F_i is the force due to interfacial friction, F_p is the force due to plowing (as in plastic deformation), and F_v is the force due to viscoelastic dissipation (as with rubber friction). There are other many other sources that have been established or postulated, including electronic dissipation[12,13] and phononic friction.[14−17]

For many kinds of nanoscale single-asperity contacts in the wearless regime, one major contribution to friction is interfacial friction F_i, whereby[18]

* Corresponding author. E-mail: carpick@seas.upenn.edu.
† University of Wisconsin−Madison.
§ Auburn University.
‡ Present address: Department of Physics, Luther College, 700 College Drive, Decorah, Iowa 52101.
# Present address: Department of Mechanical Engineering and Applied Mechanics, University of Pennsylvania, 220 S. 33rd Street, Philadelphia, PA 19104.

(1) Ulman, A. *Introduction to Ultrathin Organic Films from Langmuir−Blodgett to Self-Assembly*; Academic Press: New York, 1991.
(2) Ulman, A. *Chem. Rev.* **1996**, *96*, 1533−1554.
(3) Srinivasan, U.; Houston, M. R.; Howe, R. T.; Maboudian, R. *J. Microelectromech. Syst.* **1998**, *7*, 252−260.
(4) Flater, E. E.; Corwin, A. D.; de Boer, M. P.; Carpick, R. W. *Wear* **2006**, *260*, 580−593.
(5) Wang, Y. *Appl. Phys. Lett.* **2004**, *85*, 5736−5738.
(6) Maboudian, R.; Ashurst, W. R.; Carraro, C. *Sens. Actuators, A* **2000**, *82*, 219−223.
(7) Maboudian, R.; Ashurst, W. R.; Carraro, C. *Tribol. Lett.* **2002**, *12*, 95−100.
(8) de Boer, M. P.; Knapp, J. A.; Michalske, T. A.; Srinivasan, U.; Maboudian, R. *Acta Mater.* **2000**, *48*, 4531−4541.
(9) de Boer, M. P.; Luck, D. L.; Ashurst, W. R.; Maboudian, R.; Corwin, A. D.; Walraven, J. A.; Redmond, J. M. *J. Microelectromech. Syst.* **2004**, *13*, 63−74.
(10) Kim, H. I.; Koini, T.; Lee, T. R.; Perry, S. S. *Langmuir* **1997**, *13*, 7192−7196.
(11) Salmeron, M. *Tribol. Lett.* **2001**, *10*, 69−79.
(12) Persson, B. N. J.; Volokitin, A. I. *J. Chem. Phys.* **1995**, *103*, 8679−8683.
(13) Tomassone, M. S.; Widom, A. *Phys. Rev. B* **1997**, *56*, 4938−4943.
(14) Tomassone, M. S.; Sokoloff, J. B.; Widom, A.; Krim, J. *Phys. Rev. Lett.* **1997**, *79*, 4798−4801.

10.1021/la063644e CCC: $37.00
Published on Web 07/27/2007

$$F_i = \tau A \quad (2)$$

where τ is the shear strength of the interface, and A is the true contact area. Note that, for a given pair of materials under given conditions, τ may be a constant or it may depend upon load. The contact area A depends on load, asperity geometry (size and shape), adhesion (interatomic forces), and the mechanical properties of the materials in contact. Equation 2 indicates that interfacial friction mechanisms may be categorized into two contributions: the intrinsic frictional resistance of the materials in contact, embodied in the shear strength τ, and the size of the interface, governed by the contact area A. The shear strength can be thought of as the friction force per interfacial atom or interfacial molecule, while the contact area represents the number of atoms or molecular groups in contact.

By way of review, we focus here on the behavior of nanoscale single-asperity contacts that occur between the tip and sample in atomic force microscope (AFM) measurements. It should be noted that numerous experiments have been performed on SAMs and other organic thin films using the surface forces apparatus (SFA),[19−24] but because of much larger lateral contact sizes, we shall not discuss the SFA measurements here.

Let us specifically consider the effect of packing density on interfacial SAM friction. Defects, such as gauche defects in the chains or vacancies in the SAM, tend to increase friction.[25−30] The number of defects present in a SAM depends on the local ordering and packing density of the film, which is correlated with monolayer properties such as chain length, substrate attachment, and deposition conditions. The effect of packing density and local order on friction has been studied experimentally in various ways.[25−28] Molecular dynamics simulations have also been used to directly study the effect of packing density.[29,30] For example, Mikulski et al. studied alkane chains on diamond, comparing fully packed configurations with a monolayer with 30% of the chains removed and observed that decreased packing density was correlated with increased friction.[29]

The contact properties for SAM interfaces, including contact area (A), contact stresses, interfacial displacements, and their variations with load, are dictated by interfacial adhesion (interatomic forces), material (tip, substrate, and monolayer) stiffnesses, film thickness, and the tip shape. The stiffness of the monolayer is the most critical stiffness since it is significantly lower than the tip and substrate stiffnesses. Monolayer stiffness is affected by the molecular composition, chain length, and packing density. Packing density may also influence friction by changing the effective contact area, that is, the number of SAM molecules in contact with the tip. The work of adhesion for interfaces with SAMs also depends on their packing density and the terminal group of the SAM molecules.[31−38]

Continuum mechanics theories, such as the Johnson−Kendall−Roberts (JKR)[39] or Derjaguin−Muller−Toporov (DMT)[40] theories, have been used to infer the interfacial contact area for AFM friction measurements. When surface forces are short range compared to the resulting elastic deformations (i.e., compliant materials, large sphere radii, and strong, short-range adhesion forces), the JKR model accurately describes contact area. The opposite limit (i.e., stiff materials, small sphere radii, and weak, long-range adhesion forces) corresponds to the DMT regime. It is also possible to model the material behavior between these two extremes using a non-dimensional physical parameter. There are several such parameters that describe this transition, including Tabor's parameter,[41,42] Maugis' parameter,[43] and the Carpick−Ogletree−Salmeron (COS) transition parameter.[44] Tabor's parameter and Maugis' parameter are physically equivalent and, within a numerical factor close to 1, correspond to the ratio of the normal elastic deformation caused by adhesion (i.e., in the absence of applied load) to the spatial range of the adhesion forces themselves. If the value of Maugis' parameter is greater than 5, the JKR model applies, whereas, if Maugis' parameter is less than 0.1, the DMT model applies. Between these values, the interfacial behavior is said to be in the transition regime. The COS parameter was empirically determined from the Maugis' transition equations[43] and ranges from 0 to 1, where 0 is DMT-like behavior and 1 is JKR-like behavior.[44]

Strikingly good agreement between the shape of friction versus load measurements and the contact area versus load dependence predicted by these theories has been observed in several cases,[18,45,46] strongly indicating that interfacial friction is occurring with a load-independent shear strength. However, the continuum models must be used cautiously, with attention paid to the appropriate limits and assumptions they entail. Specifically, these models assume that materials in contact are homogeneous, isotropic, linear elastic materials. Continuum-based modifications to account for deviations from these assumptions do exist. However, continuum mechanics may break down altogether, and recent molecular dynamics results indicate that, while the functional form of both friction and contact area versus load may

(15) Dayo, A.; Krim, J. *Int. J. Thermophys.* **1998**, *19*, 827−834.
(16) Buldum, A.; Leitner, D. M.; Ciraci, S. *Phys. Rev. B* **1999**, *59*, 16042−16046.
(17) Persson, B. N. J.; Tosatti, E.; Fuhrmann, D.; Witte, G.; Woll, C. *Phys. Rev. B* **1999**, *59*, 11777−11791.
(18) Carpick, R. W.; Agraït, N.; Ogletree, D. F.; Salmeron, M. *J. Vac. Sci. Technol. B* **1996**, *14*, 1289−1295.
(19) Briscoe, B. J.; Evans, D. C. B. *Proc. R. Soc. London, Ser. A* **1982**, *380*, 389−407.
(20) Homola, A. M.; Israelachvili, J. N.; McGuiggan, P. M.; Gee, M. L. *Wear* **1990**, *136*, 65−83.
(21) Reiter, G.; Demirel, A. L.; Peanasky, J.; Cai, L. L.; Granick, S. *J. Chem. Phys.* **1994**, *101*, 2606−2615.
(22) Klein, J.; Kumacheva, E.; Mahalu, D.; Perahia, D.; Fetters, L. J. *Nature* **1994**, *370*, 634−636.
(23) Hu, Y.-Z.; Granick, S. *Tribol. Lett.* **1998**, *5*, 81−88.
(24) Maeda, N.; Chen, N.; Tirrell, M.; Israelachvili, J. N. *Science* **2002**, *297*, 379−382.
(25) Xiao, X.; Hu, J.; Charych, D. H.; Salmeron, M. *Langmuir* **1996**, *12*, 235−237.
(26) Lio, A.; Charych, D. H.; Salmeron, M. *J. Phys. Chem. B* **1997**, *101*, 3800−3805.
(27) Brewer, N. J.; Foster, T. T.; Leggett, G. J.; Alexander, M. R.; McAlpine, E. *J. Phys. Chem. B* **2004**, *108*, 4723−4728.
(28) Lee, S.; Young-Seok, S.; Colorado, R., Jr.; Guenard, R. L.; Lee, T. R.; Perry, S. S. *Langmuir* **2000**, *16*, 2220−2224.
(29) Mikulski, P. T.; Harrison, J. A. *J. Am. Chem. Soc.* **2001**, *123*, 6873−6881.
(30) Chandross, M.; Webb, E. B.; Stevens, M. J.; Grest, G. S.; Garofalini, S. H. *Phys. Rev. Lett.* **2004**, *93*, 166103.
(31) Ahn, H.-S.; Cuong, P. D.; Park, S. *Wear* **2003**, *255*, 819−825.
(32) Ashurst, W. R.; Yau, C.; Carraro, C.; Maboudian, R.; Dugger, M. T. *J. Microelectromech. Syst.* **2001**, *10*, 41−49.
(33) Ashurst, W. R.; Yau, C.; Carraro, C.; Lee, C.; Kluth, G. J.; Howe, R. T.; Maboudian, R. *Sens. Actuators, A* **2001**, *91*, 239−248.
(34) Mayer, T. M.; de Boer, M. P.; Shinn, N. D.; Clews, P. J.; Michalske, T. A. *J. Vac. Sci. Technol., B* **2000**, *18*, 2433−2440.
(35) Zhang, L.; Li, L.; Chen, S.; Jiang, S. *Langmuir* **2002**, *18*, 5448−5456.
(36) Burns, A. R.; Houston, J. E.; Carpick, R. W.; Michalske, T. A. *Langmuir* **1999**, *15*, 2922−2930.
(37) Chandross, M.; Grest, G. S.; Stevens, M. J. *Langmuir* **2002**, *18*, 8392−8399.
(38) Park, B.; Chandross, M.; Stevens, M. J.; Grest, G. S. *Langmuir* **2003**, *19*, 9239−9245.
(39) Johnson, K. L.; Kendall, K.; Roberts, A. D. *Proc. R. Soc. London, Ser. A* **1971**, *324*, 301−313.
(40) Derjaguin, B. V.; Muller, V. M.; Toporov, Y. P. *J. Colloid Interface Sci.* **1975**, *53*, 314−326.
(41) Tabor, D. *J. Colloid Interface Sci.* **1977**, *58*, 2−13.
(42) Greenwood, J. A. *Proc. R. Soc. London, Ser. A* **1997**, *453*, 1277−1297.
(43) Maugis, D. *J. Colloid Interface Sci.* **1992**, *150*, 243−269.
(44) Carpick, R. W.; Ogletree, D. F.; Salmeron, M. *J. Colloid Interface Sci.* **1999**, *211*, 395−400.
(45) Carpick, R. W.; Agraït, N.; Ogletree, D. F.; Salmeron, M. *Langmuir* **1996**, *12*, 3334−3340.
(46) Carpick, R. W.; Salmeron, M. *Chem. Rev.* **1997**, *97*, 1163−1194.

resemble the continuum solutions, the actual values are in significant error.[47,48]

Regarding continuum-based modifications, of particular interest are contact problems where one or both of the surfaces are coated with a compliant layer that represents a SAM coating. There have been several attempts to extend the applicability of these models, both analytically and computationally, to problems involving an elastic, layered substrate.[49−55] Sridhar et al. investigated deviations from the JKR model for a thin compliant layer on an elastic substrate with a rigid paraboloidal indenter. They found that, depending on an adhesion parameter that involves the work of adhesion γ, film thickness, film modulus, and indenter radius R, the pull-off force L_c varies between $-1.5\pi\gamma R$ and $-2.85\pi\gamma R$.[53] Another recent method has shown that the absolute value of the pull-off force for a material with JKR-like coating can be higher than that for the homogeneous case. Specifically, the pull-off forces for JKR-like and DMT-like coatings were identical ($-2\pi\gamma R$).[55] Although these two models give differing predictions on the pull-off force, both indicate that the pull-off force differs from what is predicted by purely homogeneous models, which makes appropriate calculation of the work of adhesion challenging.

An additional method to characterize the contact area is through the contact stiffness. Contact stiffness can be probed either normally (normal stiffness) or laterally (lateral stiffness). The normal contact stiffness of a Hertzian contact is

$$k_{\text{contact}} = 2E^*a \tag{3}$$

where a is the contact radius, $E^* = [(1 - \nu_1^2)/E_1 + (1 - \nu_2^2)/E_2]^{-1}$, E_1 and E_2 are the Young's moduli, and ν_1 and ν_2 are the Poisson's ratios of the two materials in contact. Similarly, the lateral contact stiffness is

$$\kappa_{\text{contact}} = 8G^*a \tag{4}$$

where $G^* = [(1 - \nu_1)/G_1 + (1 - \nu_2)/G_2]^{-1}$, and G_1 and G_2 are the shear moduli of the two materials. Equation 4 applies to both non-adhesive (Hertzian) and adhesive contacts, and both equations assume homogeneous, isotropic, linear, elastic materials. By modulating the contact normally or laterally, one can determine the respective contact stiffness,[56−60] and this provides insight into the variation of the contact area and the elastic response as a function of load.

Understanding the tribology of organic monolayers is further complicated by considering nonlinear and time-dependent (viscoelastic) material behavior. For example, evidence for time-dependent behavior has been observed for submicron-thick layers of polystyrene and polyvinyl benzyl chloride.[24] Nonlinear elastic behavior of alkanethiols under compression has been reported experimentally.[61] Kiely and Houston measured friction between an interfacial force microscope (IFM) tungsten tip and alkanethiols on Au as a function of load and velocity and were able to model their data using linear viscoelasticity and a standard linear solid model.[62]

As well, at the nanometer scale, organic molecules may behave in ways that simply cannot be described by continuum mechanics. As mentioned above, Luan and Robbins predict that, even for simple solids, the atomic-scale roughness of tips with radii even as large as 30 nm may cause significant deviations from continuum predictions for the contact area and pressure distribution for the contact.[47] This indicates that continuum-based models may not be correct at small scales. The idea of contact area itself may break down entirely at small scales due to complexities associated with the very definition of contact, especially for surfaces interacting under long-range van der Waals forces.[42]

Therefore, while significant progress has been made to elucidate mechanisms of SAM friction, questions remain. Previous frictional studies on SAMs have rarely been performed using self-mated interfaces, and controlled experiments comparing mated with unmated interfaces are also lacking. There has been no systematic comparison of the effect of coating the tip versus coating the substrate. Most studies have only looked at friction, and have not included stiffness measurements.[27,63−66] The relationship between film stiffness, contact area, and friction and particularly whether interfacial friction is the dominant contribution are subjects that have not been addressed. As well, few studies have included tip characterization and experimental calibration of forces. Here, we study both unmated and self-mated interfaces in order to determine the effect of coating the tip, the substrate, or both. We also present lateral contact stiffness measurements alongside with friction measurements on octadecyltrichlorosilane (OTS) to further elucidate the mechanical response of the interface. This work is also distinct because of the rigorous calibration and characterization methods used.

Materials and Methods

OTS (sometimes referred to as ODTS in the literature) monolayer films are of particular interest because they have been extensively used for coating MEMS devices. The schematic in Figure 1 shows the precursor molecule and several molecules attached to silicon oxide. This figure shows multiple possible bonding configurations of the OTS molecules, such as chemisorption, physisorption, hydrogen bonding, and short-range cross-linking between the molecules. The exact state of the bonding of OTS molecules to the surface and to other OTS molecules is not fully determined, but it has been shown that complete and continuous lateral cross-linking of OTS is sterically forbidden.[67]

The OTS monolayers were created on rigorously cleaned surfaces using liquid deposition.[6] Surface cleaning of Si(100) samples consisted of sonication in acetone for 5 min and drying in nitrogen. The samples were then exposed to an RF oxygen plasma generated by capacitively coupled titanium electrodes inside a vacuum chamber. Plasma conditions were approximately 300 mTorr O_2 at 15 W forward power for 5 min. After plasma cleaning, water contact angles are verified to be less than 3° using a Rame-Hart model 200-A contact angle goniometer. Typically, full wetting is achieved. The samples are then etched of their oxide layer in concentrated aqueous

(47) Luan, B.; Robbins, M. O. *Nature* **2005**, *435*, 929−932.
(48) Luan, B.; Robbins, M. O. *Phys. Rev. E* **2006**, *74*, 026111.
(49) Johnson, K. L.; Sridhar, I. *J. Phys. D* **2001**, *34*, 683−689.
(50) Hsueh, C.-H.; Miranda, P. *J. Mater. Res.* **2004**, *19*, 94−100.
(51) Perriot, A.; Barthel, E. *J. Mater. Res.* **2004**, *19*, 600−608.
(52) Hsueh, C.-H.; Miranda, P. *J. Mater. Res.* **2004**, *19*, 2774−2781.
(53) Sridhar, I.; Zheng, Z. W.; Johnson, K. L. *J. Phys. D* **2004**, *37*, 2886−2895.
(54) Wang, M.; Liechti, K. M.; Srinivasan, V.; White, J. M.; Rossky, P. J.; Stone, M. T. *J. Appl. Mech.* **2006**, *73*, 769−777.
(55) Reedy, E. D., Jr. *J. Mater. Res.* **2006**, *21*, 2660−2668.
(56) Lantz, M. A.; O'Shea, S. J.; Welland, M. E.; Johnson, K. L. *Phys. Rev. B* **1997**, *55*, 10776−10785.
(57) Lantz, M. A.; O'Shea, S. J.; Hoole, A. C. F.; Welland, M. E. *Appl. Phys. Lett.* **1997**, *70*, 970−972.
(58) Carpick, R. W.; Ogletree, D. F.; Salmeron, M. *Appl. Phys. Lett.* **1997**, *70*, 1548−1550.
(59) Piétrement, O.; Beaudoin, J. L.; Troyon, M. *Tribol. Lett.* **1999**, *7*, 213−220.
(60) Piétrement, O.; Troyon, M. *Langmuir* **2001**, *17*, 6540−6546.
(61) Houston, J. E.; Doelling, C. M.; Vanderlick, T. K.; Hu, Y.; Scoles, G.; Wenzl, I.; Lee, T. R. *Langmuir* **2005**, *21*, 3926−3932.
(62) Kiely, J. D.; Houston, J. E. *Langmuir* **1999**, *15*, 4513−4519.
(63) Green, J.-B. D.; McDermott, M. T.; Porter, M. D.; Siperko, L. M. *J. Phys. Chem.* **1995**, *99*, 10960−10965.
(64) Wei, Z. Q.; Wang, C.; Bai, C. L. *Surf. Sci.* **2000**, *467*, 185−190.
(65) Brewer, N. J.; Beake, B. D.; Leggett, G. J. *Langmuir* **2001**, *17*, 1970−1974.
(66) Major, R. C. *Tribol. Lett.* **2003**, *14*, 237−244.
(67) Stevens, M. J. *Langmuir* **1999**, *15*, 2773−2778.

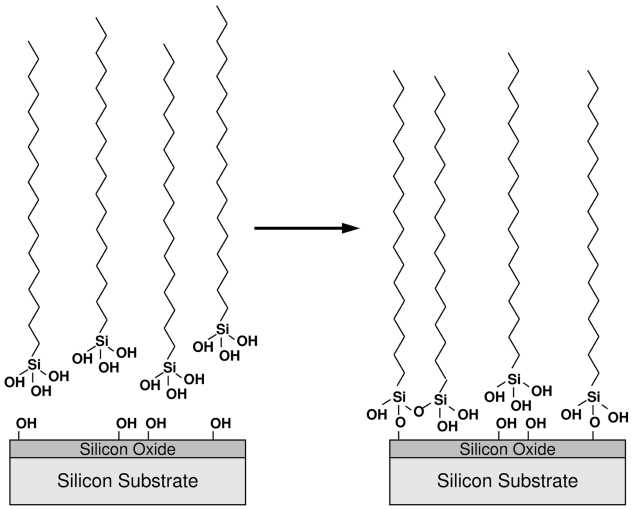

Figure 1. A schematic of OTS molecules and their attachment to a silicon oxide surface. Although the exact bonding details of OTS are not known, it is probable that the molecules either physisorb or chemisorb to the silicon oxide, and some of the molecules form short-range cross-linked structures.

hydrofluoric acid (HF) for 5 min and rinsed quickly with water and dried in nitrogen. The plasma/HF/water process is repeated at least three times, and after the third, a sample is inspected with AFM for particles. Typically, no particles are found within a $10 \times 10\ \mu m^2$ scan. The root-mean-square (rms) roughness of Si(100) cleaned in this manner is less than 0.2 nm over a $10 \times 10\ \mu m^2$ scan.

Due to concern over the preservation of tip geometry, a different cleaning procedure was used for the AFM cantilevers. Instead of repeatedly oxidizing and etching, a single exposure to a low power (1 W forward) oxygen plasma at 250 mTorr for 5 min was used. These conditions were verified to produce fully wettable Si(100) surfaces by starting with pre-cleaned samples that have aged several days under laboratory ambient conditions (and therefore became contaminated with adventitious hydrocarbons).

The OTS coating process is immediately performed on cleaned samples. The OTS solution consists of a 1 mmol solution of OTS in hexanes (Fisher, technical grade). The OTS is >97% *n*-C18 from Gelest. The solution is allowed to sit under ambient conditions ($T = 22$ °C, RH = 40%) covered for 30 min before insertion of the samples. Samples are exposed to the OTS solution for approximately 20 min and rinsed at least three times in hexanes before drying in nitrogen.

To produce well-defined counterfaces for the experiments, as well as to closely mimic and compare to MEMS devices, silicon substrates, silicon AFM tips, and silicon MEMS friction test devices[9] were coated simultaneously with the OTS monolayers. This paper discusses the nanoscale friction results using the silicon substrates and silicon tips. Note that all Si surfaces are expected to have a ~1.5 nm thick native oxide present. For simplicity, we refer to the material as "Si" even though the surfaces are silicon oxide.

All AFM data were obtained using a Veeco (Santa Barbara, CA) MultiMode AFM with a Nanoscope IV controller. The EV scanner (maximum in-plane scan range of 12 μm) used for the experiments was calibrated in *x*, *y*, and *z* using silicon micromachined calibration gratings. Silicon rectangular contact-mode cantilevers (MikroMasch, Tallinn, Estonia) were calibrated experimentally for normal forces using the Sader unloaded resonance method[68] and calibrated for lateral forces using the wedge calibration method.[69,70] The *Q* factor, which is needed for the Sader method, was obtained from the resonance curve of the cantilever, where *Q* is the resonance frequency divided by the full width at $1/\sqrt{2}$ of the maximum of the peak.

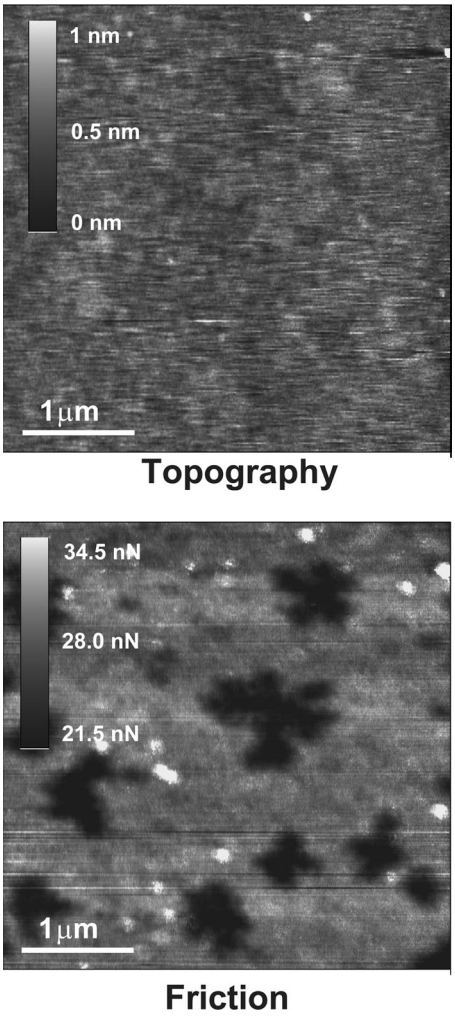

Figure 2. AFM images of OTS-coated single-crystal silicon with native oxide. The top image is topography and the bottom image is friction. Both images show the presence of dendritic regions with slightly higher topography and lower friction, which constitute the more dense LC phase. The LE phase surrounds the LC regions and is less dense. This 512×256 pixel image was scanned at nominally zero load at 1.0 Hz.

Optical microscopy was used to measure the in-plane dimensions of the lever, namely, length and width, and transmission electron microscopy (TEM) was used to measure the small critical dimensions of the cantilevers, such as tip radius, tip height, and lever thickness. The tip shape was determined using TEM.[71−74] TEM images were taken using either a JEOL 100CX or a JEOL 200CX (Tokyo, Japan), with resolution for high-magnification tip images of approximately 3 nm. The radius of the tip was determined by a fitting a circle to the end of the tip. Friction versus load (FvL) data are obtained by continuously varying the setpoint using a triangle-wave form from an external function generator at a rate of 5.86 mHz, so that one period of the triangle-wave is traversed exactly once during a 512-line image scanned at 3.05 lines/s. The load is ramped as the tip scans to create 512×512 pixel images of both normal force and lateral force.

A representative AFM image of the OTS-coated surface is shown in Figure 2. The surface has very low roughness (0.1 nm rms for this $4 \times 4\ \mu m^2$ image). However, the surface exhibits dendritic formations in both topography and friction. The nature of this contrast

(68) Sader, J. E.; Chon, J. W. M.; Mulvaney, P. *Rev. Sci. Instrum.* **1999**, *70*, 3967−3969.
(69) Ogletree, D. F.; Carpick, R. W.; Salmeron, M. *Rev. Sci. Instrum.* **1996**, *67*, 3298−3306.
(70) Varenberg, M.; Etsion, I.; Halperin, G. *Rev. Sci. Instrum.* **2003**, *74*, 3362−3367.
(71) DeRose, J. A.; Revel, J.-P. *Microsc. Microanal.* **1997**, *3*, 203−213.
(72) Schwarz, U. D.; Zworner, O.; Koster, P.; Wiesendanger, R. *J. Vac. Sci. Technol., B* **1997**, *15*, 1527−1530.
(73) Erts, D.; Lohmus, A.; Lohmus, R.; Olin, H.; Pokropivny, A. V.; Ryen, L.; Svensson, K. *Appl. Surf. Sci.* **2002**, *188*, 460−466.
(74) Fujisawa, S.; Kizuka, T. *Jpn. J. Appl. Phys. 2* **2003**, *42*, L1182−L1184.

will be discussed in detail further below. For newly deposited substrates, the dendritic patterns were not evident initially, but as loosely bound material was swept away by the tip during imaging, the patterns readily became apparent. This loose contamination, which is likely unbound OTS molecules remaining from the deposition, was typically removed after five to six imaging scans at zero applied load. Two weeks after deposition, this loose material was no longer observed. The dendritic patterns were seen regardless of the tip used or whether the tip was coated with OTS. The friction force in the dendritic regions can be 10−70% lower than the surrounding regions, depending on the tip.

Precise, reproducible nanotribological measurements with AFM are challenging, and several instrumentation issues must be carefully considered to achieve consistent results on SAM films. Since the OTS surface is frictionally inhomogeneous, the precise location on the surface for friction measurements is critical. Accurate positioning while the load was ramped was achieved using tilt compensation to nearly eliminate the longitudinal displacement of the tip along the substrate's surface that otherwise would occur due to the cantilever's tilt angle.[75] Positional uncertainty due to creep of the piezoelectrics and thermal drift was characterized and compensated for by systematically returning the tip to its original location on the surface after every few scans using a fiducial image feature.

Even with carefully addressing unwanted in-plane positional displacement of the tip, measured friction and adhesion forces can vary substantially for the same substrate and tip. Several AFM studies[76−78] show that, when working with SAMs, the tip shape and chemistry can be "run-in" to an equilibrated state, which then allows for reproducible experiments. For the experiments described in this paper, each tip was first scanned for 30 min at an applied load of 65 nN on an OTS substrate to induce a moderate amount of tip modification and to equilibrate the tip chemistry. Run-in led to significantly more consistent friction measured on the OTS substrate, indicating that an equilibrated tip geometry and chemistry were obtained. This run-in is different from that which is commonly seen for macroscopic contacts. Such behavior involves significant transfer and transformation of material. However, in the case of SAMs, transfer of material occurs, at most, at the molecular scale. Such a phenomenon is extremely difficult to observe and verify directly, as no techniques for the in-situ spectroscopic imaging of nanoscale tips exist. However, the behavior seen—a modest amount of transient behavior followed by stable friction and adhesion characteristics—is consistent with this idea, as well as with previous reports in the literature.[77,78] One plausible hypothesis is that run-in removes weakly bound material from the tip.

Results and Discussion

Uncoated and Coated Tips and Substrates. As stated above, both silicon AFM tips and single-crystal silicon substrates were coated with OTS. For simplicity, the four frictional interfaces studied are labeled in the form "tip-on-substrate". Comparisons of frictional behavior were made between the following four interfaces: a Si tip sliding on a Si substrate (Si-on-Si), the same Si tip sliding on an OTS-coated substrate (Si-on-OTS), an OTS-coated tip sliding on a Si substrate (OTS-on-Si), and the same OTS-coated tip sliding on an OTS-coated substrate (OTS-on-OTS). The same tips and substrates were used in these combinations to investigate the frictional variations between the different interfaces. As discussed further below, the OTS film is heterogeneous, as it consists of two coexisting phases known as the liquid condensed (LC) and liquid expanded (LE) phases. For consistency, locations on the sample corresponding to the LC phase were chosen for study (the dependence of friction on the OTS phase was also investigated and is discussed below).

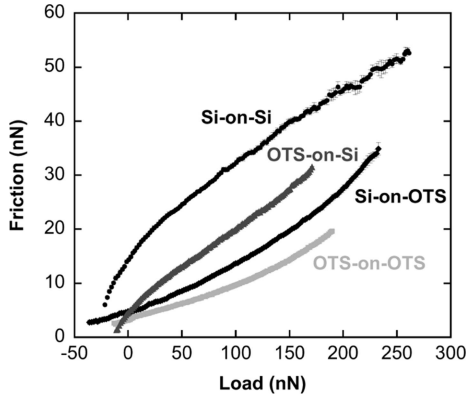

Figure 3. FvL plots of Si-on-Si, Si-on-OTS, OTS-on-Si, and OTS-on-OTS friction. Friction for Si-on-Si shows sublinear behavior, while the Si-on-OTS tip displays superlinear friction. In contrast, OTS-on-Si shows different concavity than Si-on-OTS, showing that the curvature of the SAM-coated surface plays an important role. The OTS-on-OTS friction also displays the superlinear behavior of Si-on-Si, suggesting molecular plowing behavior.

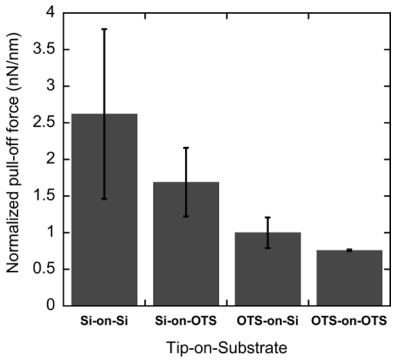

Figure 4. Normalized pull-off force, which is the pull-off force divided by the tip radius. The work of adhesion is inversely proportional to the tip radius, but the scaling factor depends on the details of the material interactions. This plot shows the relative differences in the work of adhesion between the different types of coated and uncoated interfaces. The Si-on-Si interface has the highest work of adhesion, with a large variability due to the variable surface chemistry of Si.

The phase of OTS on the tip is unknown. It has been suggested that the OTS film on nanoscale asperities may be different from the OTS film on the sample since the significant curvature of the tip may cause the chains to spread further apart than on smooth surfaces.[79] For each case, friction was first measured on the OTS-coated substrate, then measured on the bare substrate, and then back to the OTS surface to check for changes in friction. Friction on OTS was consistent when the tip was run-in prior to these experiments, as explained above.

The results are shown in Figure 3. Each data set shown is an average of the increasing and decreasing load portions of the particular FvL experiment. Averaging is feasible due the high reproducibility of the measurements. All of the error bars in the FvL plots indicate the statistically determined standard error of the mean, which means that there is 68% confidence that the true value occurs within that interval. The Si-on-Si friction curve shows the familiar sublinear behavior for a single-asperity contact exhibiting interfacial friction. The same Si tip was used to measure friction on OTS (Si-on-OTS), but it shows a different frictional response. In this case, the slope of the friction curve increases with load, which is a superlinear curve. Similarly to the case of Si-on-Si, OTS-on-Si friction varies in a sublinear manner. For

(75) Cannara, R. J.; Brukman, M. J.; Carpick, R. W. *Rev. Sci. Instrum.* **2005**, *76*, 053706.
(76) Wenzler, L. A.; Moyes, G. L.; Harris, J. M.; Beebe, T. P., Jr. *Anal. Chem.* **1997**, *69*, 2855−2861.
(77) Qian, L. M.; Xiao, X.-d.; Wen, S. Z. *Langmuir* **2000**, *16*, 662−670.
(78) Brukman, M. J.; Oncins Marco, G.; Dunbar, T. D.; Boardman, L. D.; Carpick, R. W. *Langmuir* **2006**, *22*, 3988−3998.
(79) Batteas, J. D.; Xu, C.; Helt, J.; Weldon, M. K. *ANTEC 2001 Proc.* **2001**, *2*, 1951−1954.

Table 1. Pull-off Forces and Work of Adhesion Values for Different OTS and Si Contact Pairs, as Determined by Applying Contact Mechanics Models[a]

tip/substrate	pull-off force, L_c (nN)	relative pull-off force, L_c/R (nN/nm)	work of adhesion, γ (mJ/m^2)	model for work of adhesion
Si-on-Si	63.4 ± 31.1	2.62 ± 1.16	826 ± 186	transition fit, $\alpha_{COS} = 0.56$
Si-on-OTS	38.7 ± 11.6	1.68 ± 0.47	268.1 ± 75.6	DMT
			357.5 ± 100.8	JKR
OTS-on-Si	12.9 ± 0.9	1.00 ± 0.21	159.2 ± 34.2	DMT
OTS-on-OTS	23.5 ± 11.5	0.76 ± 0.01	121.6 ± 2.2	DMT
			162.1 ± 2.9	JKR

[a] Uncertainty in the measurements was calculated using the standard error of the mean from the statistical ensemble of measurements.

OTS-on-OTS, the frictional response again gives a superlinear frictional curve.

Pull-off forces were determined from FvL plots, and these measurements were repeated using several tips and substrates. The average pull-off force values and their uncertainties are shown in Table 1. Typically, two to three pull-off force measurements are extracted from the FvL plots for each tip−sample pair and averaged. Just as in the FvL plots, the error bars represent the standard error of the mean values. Even though the exact nature of the material interactions and the validity of contact mechanics models for this system are uncertain, a *relative* comparison of the work of adhesion values is certainly meaningful, provided that the constant of proportionality between the work of adhesion and pull-off force, as explained above, does not change significantly for the four interfaces. For this reason, we present a comparison of the relative pull-off force, that is, the pull-off force normalized by the tip radius (Figure 4, Table 1). Some variations in pull-off forces occur, as seen by the differences between the example in Figure 3 and the averages in Figure 4. This may be due to premature pull-off during FvL measurements, but regardless, the trends for different interfaces are reproducible and consistent with other measurements including force versus displacement data.

The relative pull-off force is much larger for the Si-on-Si interface than for all the others. The Si-on-OTS, OTS-on-Si, and OTS-on-OTS interfaces all have similar relative pull-off forces within their 68% confidence intervals (i.e., their standard errors). It is interesting to note that the OTS-on-OTS interface has the smallest standard error, meaning it had the smallest amount of variation among the values measured. The large variation for Si-on-Si is consistent with measurements by Batteas et al.,[80] who attribute this to the spatial variations in local charge density on the oxidized silicon surface that result from local variations in the density of silanol groups.

We can use the analysis of variance (ANOVA) to determine whether there is a statistical difference in a sample measurement due to the variation of a particular variable. For the pull-off force measurements, we consider the different interfaces in terms of varying two specific variables: the tip coating and the substrate coating. By looking at the differences in all the combinations of tip and substrate, one can determine (a) whether the tip coating has an effect on pull-off force, (b) whether the substrate coating has an effect on pull-off force, or (c) whether coating the tip and coating the substrate influence each other in determining the pull-off force (e.g., if the effect due to coating both the tip and the substrate is greater than the sum of the effects of either coating the tip or coating the substrate).

The analysis shows that there is a 50% confidence level that there is a difference in pull-off force due to the tip coating, and 80% confidence that there is a difference in pull-off force due to the substrate coating. In addition, there is a lack of evidence that the tip coating and substrate coating influence one another for determining the pull-off force. This information, along with the overall low value and small confidence interval for the OTS-on-OTS pull-off force, indicates that the OTS-on-OTS interface has a high level of stability and consistency in its work of adhesion. It also implies that, for example, MEMS device performance and consistency should be improved by coating silicon MEMS surfaces with OTS. This is indeed what has been observed experimentally.[4] This is further corroborated by the fact that OTS reduces interfacial friction for single asperities (Figure 3).

These results, that the tip coating would have a significant effect on pull-off force and that the Si-on-Si interface would have the largest pull-off force, agree with expectations. The large Si-on-Si pull-off force can be attributed to the naturally hydrophilic native oxide of the bare silicon surface, which can exhibit high adhesion.[80] In this particular case, the Si surface used for Figure 3 was cleaned using First Contact, a contamination removal polymer film (Photonic Cleaning Technologies, Platteville, WI). This cleaning procedure leaves the surface free of debris and contamination according to optical microscopy and AFM topographic imaging. Certainly any substrate exposed to air will possess both water and adventitious hydrocarbon contamination. Thus, as with any other AFM measurement in air, the precise surface chemistry is unknown.

The ANOVA methodology also shows that there is 95% confidence that both the tip coating and the substrate coating have significant effects on the frictional response of the various interfaces. This was determined by comparing the values of the friction force at zero applied load for each interface. As well, there is 95% confidence that there is some interaction between the effects of the tip coating and the substrate coating. Since pull-off force and friction are both influenced by the substrate coating, the data in Figure 3 are separated according to the substrate (Figure 5). It is obvious that whether sublinear or superlinear behavior occurs for the FvL curve depends on the nature of the *substrate* (coated vs uncoated) and not the tip.

In Figure 5a, the data for Si-on-Si and OTS-on-Si are extremely well fit by a continuum mechanics model for the contact area of an elastic adhesive single asperity (solid lines) and assuming interfacial friction (eq 2) with a constant shear strength. A small deviation from the fit is seen for OTS-on-Si only at the highest loads (>140 nN). The Si-on-Si interface is fit by the COS transition model, with a COS transition parameter of 0.56, which indicates material behavior intermediate to the DMT and JKR regimes. The corresponding Maugis' parameter is 0.78. The OTS-on-Si interface, on the other hand, is best described by a purely DMT model. In contrast, the Si-on-OTS and OTS-on-OTS curves (Figure 5b) cannot be fit with any known contact mechanics model for contact area with a constant shear strength, since no models predict a superlinear behavior for a paraboloidal tip. Therefore, a range of possible work of adhesion values using the DMT and JKR values as limits are presented in Table 1 for these interfaces.

(80) Batteas, J. D.; Quan, X.; Weldon, M. K. *Tribol. Lett.* **1999**, *7*, 121−128.

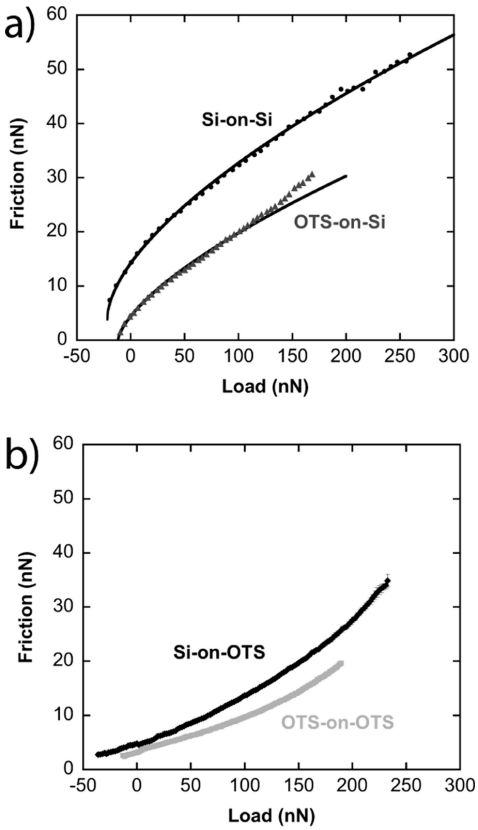

Figure 5. Friction vs load for OTS-coated and uncoated tips and substrates. The number of data points has been reduced from the plots in Figure 4 to clearly show the curve fits. (a) Frictional data for tips sliding on Si are well-described by a DMT-like model for contact area (fits shown by black lines). (b) Frictional data for tips sliding on OTS cannot be easily fit to contact mechanics models, even for a limited range of loads. Frictional behavior can be attributed to molecular plowing in the OTS film.

The shear strength τ can only be determined for Si-on-Si, since the modulus of the OTS layer is unknown. For the Si-on-Si plot in Figure 5a, which was fit using a tip radius of 15 nm (determined by TEM), and using bulk values for the elastic modulus and Poisson's ratio of Si(100),[81] the shear strength is calculated to be 1100 ± 20 MPa. The fact that this data can be fit by the COS equation is consistent with the hypothesis that continuum linear elasticity accurately describes the contact area variation with load for this interface, and that its interfacial shear strength is load-independent according to eq 2. On the basis of the fits, we can estimate that the contact radius for the Si-on-Si interface varies from 1.02 ± 0.01 nm at a pull-off load of −25.3 ± 0.7 nN to 2.83 ± 0.03 nm at 200 nN. The mean contact stresses (load divided by contact area) at these loads are −7.74 and 7.95 GPa, respectively.

The small deviation from the DMT fit for the OTS-on-Si data above 140 nN load may suggest an additional frictional contribution at the higher loads. Furthermore, while the shape of the FvL curve for OTS-coated substrates depends on the type of tip (bare, or OTS-coated) used, the common trend is that friction is nonlinear with an increasing slope as the load increases. These superlinear FvL plots could be explained in two different ways. The first explanation is that friction is still proportional to contact area (i.e., interfacial friction, $F_i = \tau A$), but with a pressure-dependent shear strength τ. If so, then the pressure dependence itself must be superlinear to compensate for the contact area increasing only sublinearly. If there was indeed a pressure-dependent shear strength when sliding over an OTS-coated surface, it would be expected that Si-on-OTS and OTS-on-Si friction should exhibit the same behavior, but this is not observed.

(81) The mechanical properties of Si used for this calculation were 150 GPa for the modulus and 0.28 for Poisson's ratio.

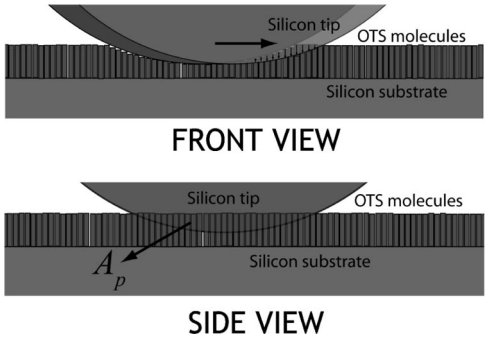

Figure 6. Cartoon illustrating a 20 nm tip plowing into OTS molecules. Because of relatively weak chain-to-chain interactions, compression of molecules under the tip has little influence on the molecules outside of the contact area. As the tip moves laterally, it plows into the molecules in front of it, which occupy the projected area A_p. The molecules in this region are compressed, bent, and/or tilted out of the way of the tip.

The second explanation is that an additional contribution to friction, independent of interfacial friction, contributes to this superlinear behavior. Here we propose one plausible mechanism, namely, molecular plowing. Because of relatively weak lateral chain−chain interactions in the SAM, the compression of molecules under the tip has reduced influence on the height of the molecules outside of the contact area (assuming vertically oriented molecules). As the tip moves laterally along the film, the tip therefore plows into the uncompressed molecules in front of it. Those molecules must be compressed toward the substrate or tilted laterally for the tip to pass through. This kinematic process is shown schematically in Figure 6, where the compression of the molecules is exaggerated to illustrate the hypothesized effect. This effect will produce a force resistive to forward motion. In a fully elastic system, the recovery of compressed or laterally displaced molecules behind the tip would compensate for this resistive force. However, thermal fluctuations, viscoelasticity (temporal delay in the elastic recovery), and other random processes involving the SAM molecules will interfere with this. Thus, a net resistive force occurs.

In this picture, the major contributions to friction for SAM systems are due to both interfacial friction and to plowing friction (i.e., $F_f = F_i + F_p$). The interfacial friction term is still proportional to the interfacial contact area ($F_i = \tau A$), while the plowing force is an unknown nonlinear function of load and contact radius ($F_p = F_p(L,a)$), such that

$$F_f = \tau A + F_p(L,a) \tag{5}$$

In other words, the two contributions to the force resisting sliding are (1) an interfacial friction force, which arises from the fact that molecular groups at the interface itself have a preferred interfacial arrangement, the shearing of which requires energy to be expended, and (2) plowing, which arises from the need to compress or displace molecules in front of the tip to move forward, which also requires energy to be expended.

Macroscopic plowing behavior in tribological contacts has been studied for decades and typically involves plastic deformation,[82] but it has been previously suggested that molecular plowing also contributes to friction for monolayer systems at the nanoscale.[78,83,84] Brukman et al. showed that, from simple geometry, the area A_p of a parabolic tip projected onto the plane normal to the scanning direction is proportional to $\sqrt{R\delta^3}$, where δ is the penetration depth of the tip into the layer. For a Hertz or DMT contact, the applied load L varies with penetration depth according to $L = (4/3)E^*\sqrt{R\delta^3}$. Note that the penetration is taken to be the compression of the interface, which involves compression of both the tip and substrate (i.e., the film). However, for Si-on-OTS, the film is far more compliant than the tip, and therefore the compression will primarily occur in the film. For OTS-on-OTS, ideally the compression should be equal for the two surfaces, but the total penetration δ still represents the amount that molecules (on either the tip or substrate) outside the contact zone must be compressed to allow sliding.

Using the above relationships between load and penetration, the projected area of contact A_p will be proportional to the applied load L, but independent of the tip radius.[78,82] In the case of an adhesive but non-DMT-like contact, the dependence of L on δ is more complex, but the dependence on radius remains weak, and so A_p is nearly proportional to L except close to the pull-off load. Similarly, if we consider the contact mechanics of a SAM as represented by a thin, non-adhesive elastic coating,[55] it can be shown that $L = \pi(RE_u/h)\delta^2$, where E_u is the uniaxial strain modulus of the thin layer and h is the thickness of the layer. Since A_p is proportional to $\sqrt{R\delta^3}$, A_p can be shown to be proportional to $L^{3/4}$, again with a weak radius dependence. We note that further work is required to determine how this analysis should be modified to include adhesive interactions.

Therefore, it is hypothesized that molecular plowing generates an additional resistive force that can be very roughly given by $F_p = \eta A_p \propto L$, where η is a constant of proportionality that has a similar connotation as τ for interfacial friction. The plowing model agrees with the observations both here and by Brukman et al. that the shape or the slope of the friction curve for a given interface is relatively insensitive to changes in the pull-off force. Changes in pull-off force are indeed observed for this work, and could be due to a change in the tip radius or in the work of adhesion during the experiment. This molecular plowing model, with a roughly linear relation between friction and load, also provides a good description of the FvL data presented by Brukman et al.[78] as well as several other papers that observe linear FvL curves for uncoated tips sliding on various SAMs.[10,28,35,85−88] For the data in Figure 5b, there is good agreement with this molecular plowing model at low loads up to ∼80 nN for Si-on-OTS and ∼250 nN for OTS-on-OTS, as the interface exhibits linear FvL curves over these load ranges.

At higher loads, the deviation from linearity is more significant and takes on a superlinear character. This cannot be explained by resorting to linear elastic contact mechanics descriptions of the contact area. However, there are other strikingly similar examples in the literature where superlinear friction has been seen at higher loads with SAMs.[25,77] For example, Xiao et al. observed that, for 8 and 18 carbon alkylsilane monolayers, the FvL shows superlinear behavior at loads above 50 nN. In addition, superlinear friction was seen by Qian et al. at loads from 30 to 90 nN. Above these superlinear regimes, the frictional behavior again becomes linear. Both of these groups attribute this to the frictional response of the underlying muscovite mica substrate, that is, the tip has penetrated the SAM and is in contact with the substrate. However, they did not propose a mechanism to explain the superlinear dependence prior to breaking through the SAM, nor did they show if the superlinear friction behavior was reversible upon reducing the load. Here we clearly see that it is reversible. We argue that the superlinear region is a reversible mechanical phenomenon that can be attributed to molecular plowing.

Superlinear behavior cannot be accounted for simply by considering the fact that the effective stiffness of the monolayer-coated Si increases with load. At high loads, the effective contact modulus E^* will increase due to increased interaction with the significantly stiffer silicon substrate and due to the expected nonlinear stiffening of the OTS molecules.[54,89] Both of these effects would cause the contact area to grow more slowly with load, and therefore, according to the interfacial friction model, the friction force should be even more strongly sublinear than the DMT or JKR (or intermediate) models predict. Considering the mechanics of the thin coating geometry does not change this conclusion.[55] However, the superlinear behavior could be explained by assuming that the nonlinear stiffening of the molecules under compression leads to a greater amount of energy required (and subsequently lost) when compressing the molecules during plowing.

The difference between the Si-on-OTS and OTS-on-Si results gives additional support for the molecular plowing hypothesis. For Si-on-OTS (Figure 5b), the molecular plowing contribution is significant at all loads. For OTS-on-Si (Figure 5a), the FvL behavior agrees well with the interfacial friction model at low loads, indicating that plowing has little influence. The deviation from the contact mechanics fit at higher loads (above ∼130 nN) may indicate that molecular plowing becomes significant in this regime. This can be explained by considering the curvature of the tip. For OTS-on-Si, the tip curvature reduces the effect of molecular plowing at low loads since the molecules on the tip just outside the contact region are already located "out of the way", i.e., vertically displaced from their neighbors in the contact region, providing a kinematic advantage to sliding. At higher loads, the OTS molecules on the tip become sufficiently compressed so that the tip molecules do require plowing. Since there is no evidence of large scale wear of the OTS after scanning at high loads (Figure 7), the majority of the deformation of the OTS molecules is recovered, with irreversible molecular deformations occurring only to a limited, unobservable extent.

The fact that molecular plowing takes place is corroborated by molecular dynamics simulations that show extreme deformation and plowing for silicon oxide tips with radii of 10 nm scanning on an OTS-coated substrate.[90]

Effect of Packing Density. Another key factor affecting the frictional properties of SAMs is their packing density. As discussed above, previous work on SAMs composed of molecules with different chemical structures (chosen so that they lead to

(82) Bowden, F. P.; Tabor, D. *Friction and Lubrication of Solids: Part I*; Oxford University Press: Oxford, U.K., 1950.
(83) Clear, S. C.; Nealey, P. F. *J. Chem. Phys.* **2001**, *114*, 2802−2811.
(84) Clear, S. C.; Nealey, P. F. *Langmuir* **2001**, *17*, 720−732.
(85) Graupe, M.; Koini, T.; Kim, H. I.; Garg, N.; Miura, Y. F.; Takenaga, M.; Perry, S. S.; Lee, T. R. *Colloids Surf., A* **1999**, *154*, 239−244.
(86) Kim, H. I.; Graupe, M.; Oloba, O.; Koini, T.; Imaduddin, S.; Lee, R. L.; Perry, S. S. *Langmuir* **1999**, *15*, 3179−3185.
(87) Kim, H. I.; Koini, T.; Lee, T. R.; Perry, S. S. *Tribol. Lett.* **1998**, *4*, 137−140.
(88) Zhang, C.; Liang, Q.; Wang, B.; Xiao, X. *J. Appl. Phys.* **2004**, *95*, 3411−3416.
(89) Kiely, J. D.; Houston, J. E.; Mulder, J. A.; Hsung, R. P.; Zhu, X. Y. *Tribol. Lett.* **1999**, *7*, 103−107.
(90) Chandross, M., Sandia National Laboratories, Albuquerque, NM. Personal communication, 2006.

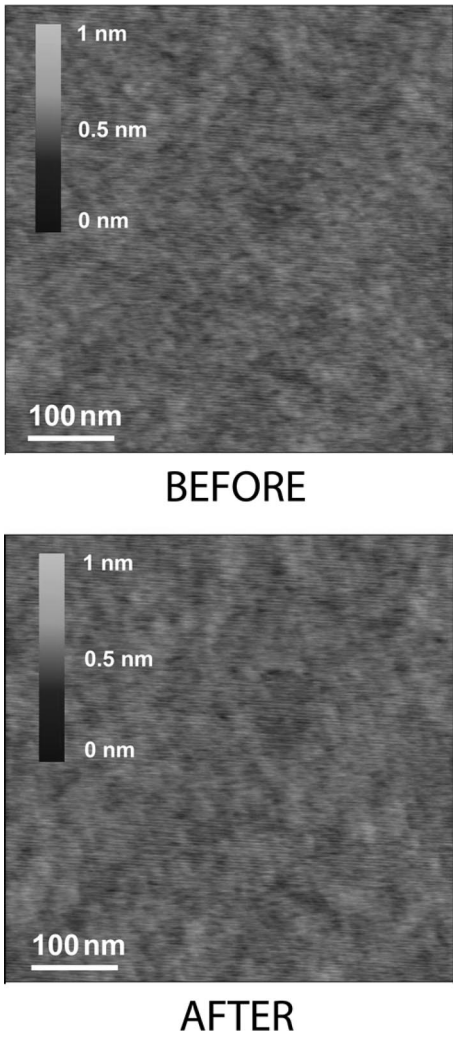

Figure 7. Representative images of OTS surface topography before and after an FvL experiment. The maximum load during this experiment was approximately 150 nN, applied over a scan range of 200 nm, in the center of this image. No observable wear is evident, and the variation in the topography of a few Angstroms is much less than the ~2.5 nm thickness of the monolayer.

different packing densities), leads to contrast in friction. Results for two *chemically identical* monolayers with different packing densities are presented here. Figure 2 shows that the OTS surface is inhomogeneous, forming dendritic patterns on the surface. This reveals the two known coexisting thermodynamic phases of the OTS monolayer, in exact agreement with those previously documented and explained by Carraro et al.[91] These same dendritic patterns have also been observed by Liu et al.[92] The dendritic formations are denoted as the denser LC phase, and the surrounding regions are the less dense LE phase. The LC phase consists of confined regions of high-density, closely packed, fully extended monolayer chains, while the LC phase consists of disordered molecules with a uniform but lower packing density. The independent observations of these types of dendritic features for OTS films demonstrates that these phases do not arise from inhomogeneities in the substrate, but from the nature of the OTS phases that form under specific deposition conditions.

We observe that the LC phase as seen in Figure 2 has slightly higher topography and significantly lower friction than the LE phase. The higher topography of the LC phase is consistent with its higher density since the tighter packing causes the molecules to orient more perpendicularly to the surface. The fact that the LE phase has higher friction than the LC phase is not surprising because, as discussed previously, decreased packing density increases friction because defects form more readily in less dense monolayers during sliding. This can increase friction in several ways, as it creates a more corrugated surface, exposes a larger fraction of methylene groups to the surface, and creates additional channels for frictional energy dissipation during sliding. The defects in the chains most likely form outside of the area of contact, where there is more free volume.

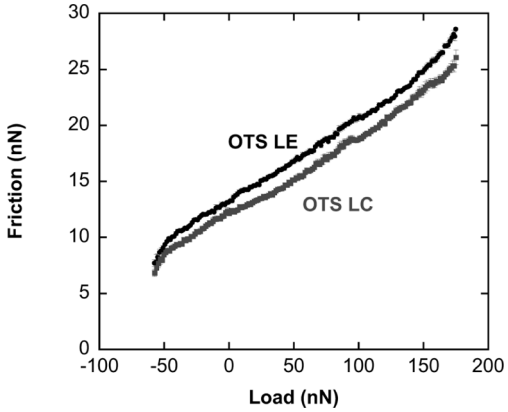

Figure 8. FvL for an OTS-coated tip on an OTS-coated substrate on the LE and LC phases. There is a modest but clear distinction between the frictional properties of the two phases over a large range of loads. Data from increasing and decreasing loads on a given phase are indistinguishable from one another and are averaged together for this plot.

It is also probable that there is an additional contribution to the frictional variation due to changes in the orientation of the tail groups of the OTS molecules within each phase. At a lower packing density, the ends of the chain are able to rotate more freely. Thus, instead of a mostly methyl-terminated interface, there would be a higher percentage of methylene groups at the interface. This has been shown in molecular dynamics simulations, whereby both the chemical identity and the orientation of the end group of a hydrocarbon chain has a significant effect on friction, with disorder, gauche defects, and methylene group exposure increasing friction.[93,94]

To definitively demonstrate the distinct frictional responses of the two phases, the FvL procedure (with tilt compensation) was performed on a region that contained both LC and LE phases side-by-side. With this approach, friction is measured repeatedly on both phases at each load for each scan line, and the location on the substrate is easily verified. In other words, we directly measure the effect of packing density variations for one specific molecule instead of comparing films composed of different molecules (e.g., with different chain lengths), which is an indirect comparison of packing density effects. The continuous fashion of acquiring comparative data within the same image completely eliminates uncertainties associated with tip, substrate, instrumental, and environmental changes.

In agreement with the friction image in Figure 2, the FvL plot in Figure 8 shows that the less dense LE phase consistently exhibits higher friction than the denser LC phase over the entire range of applied loads. The example shown in Figure 8 is for

(91) Carraro, C.; Yauw, O. W.; Sung, M. M.; Maboudian, R. *J. Phys. Chem. B* **1998**, *102*, 4441−4445.
(92) Liu, Y.; Wolf, L. K.; Messmer, M. C. *Langmuir* **2001**, *17*, 4229−4335.
(93) Mikulski, P. T.; Gao, G. T.; Chateauneuf, G. M.; Harrison, J. A. *J. Chem. Phys.* **2005**, *122*, 024701.
(94) Mikulski, P. T.; Herman, L. A.; Harrison, J. A. *Langmuir* **2005**, *21*, 12197−12206.

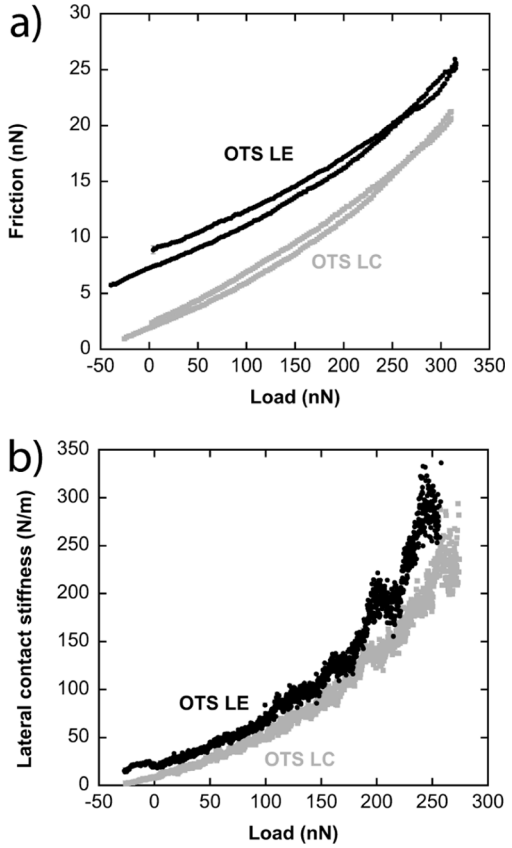

Figure 9. FvL and lateral contact stiffness of an OTS-coated tip on an OTS-coated substrate. (a) OTS-on-OTS FvL data. These data are similar to the data in Figure 6a, where the slope of the friction curve increases with load. (b) OTS-on-OTS lateral contact stiffness data. This data was taken immediately prior to each of the FvL curves shown in panel a.

an OTS-coated tip, but the contrast is also seen with uncoated tips. In this example, the offset between the LC phase and LE friction is 1−2 nN for applied loads greater than 0 nN.

The difference in friction force for the two regions is dependent on the tip used for the particular experiment, and its scanning history. For example, a different OTS-coated tip again shows higher friction for the LE phase (Figure 9a), but this time the LE phase exhibits friction forces ∼4−6 nN higher than those for the LC phase. Higher friction for the LE phase is consistently observed, but the relative difference between the phases can vary between 10 and 70%. This may be due to variability in tip structure and chemistry. The larger contrast between the LC and LE phases in Figure 9a compared to those in Figure 8 may indicate that the specific tip used has a chemical termination that is more sensitive to the friction differences of the OTS phases. The pull-off force in Figure 9a is slightly larger for the LE phase than for the LC phase, but the slopes of the FvL curves are approximately the same at a given load. Therefore, the increase in friction for the LC phase cannot be wholly attributed to the differences in adhesion between the two phases since the friction difference is much larger than the adhesion difference.

Hysteresis between increasing and decreasing load portions of the FvL curves (Figure 9a) is observed and is reproducible for this particular measurement, with friction being slightly lower when the load is being decreased. However, as seen in Figure 8, this hysteresis does not always occur. Other researchers have observed hysteresis in stiffness versus load curves for polymeric materials, but, in that case, the approach curve had lower contact stiffness than the retract curve (decreasing load), which was attributed to a viscoelastic time lag in the contact area.[95] Figure 9a, on the other hand, shows that the approach curve (increasing load) has higher friction. This effect cannot be explained by a change in the tip or the substrate during the experiment, or by spatial drift, since the curves were traced reproducibly for multiple FvL runs. It is not clear what causes this hysteretic FvL behavior, but one possible origin may be due to the plowing behavior of the molecules during these constantly varying load experiments. When the load increases during sliding, it is increasingly difficult (albeit slightly) for the viscoelastic OTS molecules to get out of the way of the tip, and this may contribute to the higher friction in the approach curve. Then, when the load decreases during sliding, the molecules have slightly more opportunity to relax and allow for the passage of the tip, which slightly reduces the resistance to sliding. Regardless of the frictional details in Figure 9a, the LE phase consistently exhibits higher friction than the LC phase, and this persists regardless of the pressure exerted on the film by the tip.

To further explore the origins of the contrast between the LC and LE phases, and to further understand the load-dependence of friction, lateral stiffness measurements[58] were also performed in the two distinct regions. The total lateral stiffness κ_{tot} measured by the cantilever will depend on the lateral contact stiffness, κ_c, the lateral stiffness of the lever, κ_l, and the lateral stiffness of the tip, κ_{tip}. It is possible to experimentally determine the torsional stiffness of the lever using the torsional Sader method,[96] but, due to overlapping normal and torsional resonances of this particular cantilever, a geometrical calculation of the torsional and lateral cantilever stiffness was performed instead. Using the measured dimensions of the lever and 60 GPa for the shear modulus of silicon, the lateral stiffness of the lever was calculated to be 127 N/m. Since the contribution of the tip's lateral stiffness can be significant,[57] this was inferred from a plot of κ_{tot}^{-1} versus $F_f^{-1/2}$, where F_f is the friction force. This value was found to be approximately 240 N/m, which corresponds well to values calculated by Lantz et al. for 30−50 nm contact-mode tips.[57]

FvL (Figure 9a) and stiffness versus load (Figure 9b) measurements for an OTS-on-OTS interface were obtained on both the LE and LC phases of the OTS sample. Although there is a clear difference in friction between LC and LE phases in Figure 9a) and all other friction measurements, the difference in lateral stiffness for the two phases is not significant. Thus, the frictional contrast between the OTS phases cannot be attributed to a difference in their elastic moduli, since this would show up as a difference in stiffness at the same load. The difference between LC and LE is not due to a contrast in contact area either, since, for the same tip and load, the contact areas should be similar since the stiffnesses are nearly the same. Furthermore, the lateral stiffness plot shows an unusual superlinear behavior, seemingly similar to that of the FvL plot. For an axisymmetric single asperity contact between linear elastic isotropic materials, contact stiffness is given by eq 4, which increases in a sub-linear manner (e.g., for a Hertz or DMT interface, the contact radius and thus the lateral stiffness increase as $L^{1/3}$). However, in Figure 9b, stiffness increases in a much more dramatic, superlinear manner. This implies that either the continuum description is not appropriate, or the contact shear modulus G^* of the contact increases with load. This can occur either due to nonlinear elasticity (stiffening) of the SAM at higher loads, or due to an increased amount of sampling of the stiffer substrate at higher loads. Since a superlinear stiffness is observed, stiffening of the contact region should lead

(95) Wahl, K. J.; Stepnowski, S. V.; Unertl, W. N. *Tribol. Lett.* **1998**, *5*, 103−107.
(96) Green, C. P.; Lioe, H.; Cleveland, J. P.; Proksch, R.; Mulvaney, P.; Sader, J. E. *Rev. Sci. Instrum.* **2004**, *75*, 1988−1996.

to a *reduction* in the rate of increase of contact area, and should therefore render interfacial friction more strongly sublinear. Since the opposite is observed, it supports the hypothesis that there is an additional friction contribution beyond interfacial friction.

As discussed in the previous section, one possibility is that the higher the load, the more difficult it is for the tip to move through the monolayer, and thus the molecular plowing contribution to friction increases drastically with load. This is equivalent to saying that the monolayer has a nonlinear viscoelastic character, and the storage and loss moduli both increase at higher stresses. The effects of nonlinear stiffness and the possibility of molecular plowing make it difficult to analyze these results in further detail without comparison to molecular dynamics simulation results. This work is in progress.

The effective modulus of the Si-on-OTS contact can indeed be influenced by the substrate at high penetration depths. The effect of the substrate on the measured monolayer stiffness was demonstrated by Kiely et al. for IFM experiments.[89] The IFM is a mechanically stable local probe device that can simultaneously measure the normal force and deflection of the contact, and this enables direct measurement of interfacial forces. Friction can also be measured. Kiely et al. observed that the friction force leveled off at pressures of 2 GPa, indicating an extremely stiff interfacial contact that they interpreted as the interaction of the tip with the stiffer substrate under the monolayer. A rough estimate of the penetration depth δ can be made for the conditions studied in this paper by using the DMT model and considering the deformation of the SAM alone. For a 45 nm tip applying a load of 300 nN, assuming a modulus of 10 GPa and a Poisson's ratio of 0.4 for the monolayer, the predicted penetration depth is 3.3 nm. Since this is larger than the thickness of an OTS monolayer (2.5−2.6 nm[97,98]), the compression at these loads must cause significant elastic deformation of the underlying substrate as well. Therefore, the effective modulus of the interface increases due to an increased contribution from the stiff substrate with load.

In conclusion, the lower density LC OTS phase has lower friction than the LE OTS phase, and the difference is not due to a difference in the stiffnesses of the two phases. Rather, it is consistent with the proposed mechanism of friction whereby higher packing density decreases the propensity for defect formation and viscoelastic effects. This was shown by measuring both friction and lateral stiffness as a function of load for the two phases.

Summary

We have discussed the frictional properties of OTS monolayers, which are commonly used in MEMS to reduce adhesion and friction. Friction, adhesion, and stiffness were measured at the nanoscale using quantitative AFM techniques. The precise location of our tip is controlled using tilt compensation and drift compensation, which enables quantitative comparisons to be made between different phases of the SAM. Transfer of SAM molecules or other contaminants to uncoated tips is common, so tips are run over a sacrificial area of the substrate by applying relatively high loads for a fixed period of time during scanning to equilibrate tip geometry and chemistry. This has wider importance for the acquisition of reproducible AFM nanotribology measurements in general, and strongly suggests that AFM researchers should strive to characterize and control the chemistry and structure of their tips to obtain meaningful measurements.

Comparisons of the interfacial properties of bare and OTS-coated tips sliding on bare and OTS-coated substrates were performed. The pull-off force and thus the work of adhesion varied from tip to tip, and varied most significantly for the Si-on-Si interface. Despite this, it was clearly demonstrated that adhesion is reduced by nearly a factor of 5 by coating the tip, substrate, or both with OTS. Tips sliding on Si, regardless of their functionality, showed the familiar sublinear single-asperity interfacial friction behavior, while tips sliding on OTS exhibited superlinear FvL behavior. This is consistent with the hypothesis that the additional contribution to friction is kinematically required plowing of the SAM molecules.

For the two phases of the OTS-coated surfaces, the LC phase shows measurably lower friction than the LE phase for a large range of loads, demonstrating that lower friction is associated with higher packing density of the molecules. The difference in friction varies with the particular tip used, but ranges from a 10 to 70% increase for the LE phase. Lateral stiffness measurements demonstrate stiffening of the interface due to nonlinear elasticity of the molecules and/or interaction with the stiffer substrate. This establishes that the packing density contrast arises from an intrinsic difference in the frictional response of the LE and LC regions, not from a difference in the elastic properties of the contact. Further work, including molecular dynamics simulations, is required to clearly elucidate the relationship between monolayer structure, viscoelasticity, and friction.

Acknowledgment. E.E.F. acknowledges the financial assistance of a National Science Foundation graduate research fellowship. This work was supported by the U.S. Department of Energy, BES-Materials Sciences, under Contract DE-FG02-02ER46016 and by Sandia National Laboratories. Sandia is a multiprogram laboratory operated by Sandia Corporation, a Lockheed Martin Company, for the U.S. Department of Energy under contract DE-AC04-94AL85000.

LA063644E

(97) Fujii, M.; Sugisawa, S.; Fukada, K.; Kato, T.; Shirakawa, T.; Seimiya, T. *Langmuir* **1994**, *10*, 984−987.

(98) Peters, R. D.; Nealey, P. F.; Crain, J. N.; Himpsel, F. J. *Langmuir* **2002**, *18*, 1250−1256.